condensed matter

MDPI

Article

Scaling between Superfluid Density and T_c in Overdoped $La_{2-x}Sr_xCuO_4$ Films

Evandro V. L. de Mello

Department de Física, Universidade Federal Fluminese, 24210-346 Niterói, RJ, Brazil; evandro@if.uff.br; Tel.: +55-21-999-253-843

Received: 19 April 2019; Accepted: 4 June 2019; Published: 6 June 2019

Abstract: We used an electronic phase separation approach to interpret the scaling between the low-temperature superfluid density average $\rho_{sc}(0)$ and the superconducting critical temperature T_c on overdoped $La_{2-x}Sr_xCuO_4$ films. Guided by the observed nematic and incommensurate charge ordering (CO), we performed simulations with a free energy that reproduces charge domains with wavelength λ_{CO} and provides a scale to local superconducting interactions. Under these conditions a complex order parameter with amplitude $\Delta_d(r_i)$ and phase $\theta(r_i)$ may develop at a domain i. We assumed that these domains are coupled by Josephson energy $E_J(r_{ij})$, proportional to the local superfluid density $\rho_{sc}(r_{ij})$. Long-range order occured when the average $E_J(T_c)$ is $\sim k_B T_c$. The linear $\rho_{sc}(0)$ vs. T_c relation was satisfied whenever CO was present, even with almost vanishing charge amplitudes.

Keywords: cuprate superconductores; electronic phase separation; superfluid density; Josephson effects

1. Introduction

Overdoped high-temperature cuprate superconductors have been widely believed to be described by the physics of d-wave BCS-like superconductivity. However, recent measurements [1] indicate that as the doping is increased, the superfluid density decreases smoothly to zero rather than increasing as expected by BCS theory in the absence of disorder. The authors in [1] developed a technique to grow homogeneous overdoped $La_{2-x}Sr_xCuO_4$ (LSCO) films and measured the penetration depth from which $\rho_{sc}(0)$ is derived, establishing a new unforeseen scaling law: $\rho_{sc}(p, T \sim 0\ \mathrm{K})$ is directly proportional to $T_c(p)$, both being maximum at $p = 0.16$ and vanishing near the superconducting (SC) limiting phase at $p = 0.26$. Their films displayed homogeneous properties with less than 1% variations in T_c [1,2], but the induction of an anisotropic transverse voltage [3] indicates some intrinsic electronic disorder.

This anisotropic transport is compatible with a nematic order, and this is another manifestation of the ubiquitous CO in cuprates [4]. In fact, the presence of bulk magnetic excitation from low to high doping [5–7] suggests the presence of either static or correlated charge fluctuations in time and space with local antiferromagnetic (AF) order that decreases with doping [6,7]. Concomitantly, the very low normal state residual resistance measured in the same experiment [1] and subsequent time-domain THz spectroscopy [8] ruled out an approach based on the dirty BCS scenario [9].

2. Results

Competing broken symmetry states in cuprates arising from a nanoscale electronic phase separation have been predicted by many different microscopic models using Hubbard, Holstein, t-J Hamiltonians, and with many different techniques [10–13]. All these models predict different forms of charge disorder such as stripes, CO, or charge density waves (CDWs) under distinct phase diagram

parameters. These fundamental calculations are essential to demonstrate that phase separation is a real phenomenon of high-T_c superconductors, but they do not reproduce the fine structure of the observed charge wavelength λ_{CO} as a function of hole-doping p that has been generally observed [4,14,15]. For exactly this purpose, we performed electronic phase separation calculations [16–20] based on the Cahn–Hilliard (CH) nonlinear differential equation [21]. The main achievement of our work lies in almost exactly mimicking the CO structure details, that is $\lambda_{CO}(p)$, and this was accomplished through the parameters involved in the CH equation and by stopping the simulation at fixed times. Although this is artificial, it is the only way to obtain the charge density maps $p(\mathbf{r})$ on the CuO plane close to the observed modulations. The approach also has the great advantage of concomitantly providing the free energy map, which leads to the superconducting interaction, as will be explained below.

Concerning the superconducting (SC) properties, there is evidence [22–24] in favor of a model exploring the similarities between the CDW alternating charge domains with a granular superconductor in which SC grains are coupled via Josephson tunneling [25,26]. We used this approach, developed mainly in [18,26], to study the superfluid and T_c scaling relation.

Therefore, we started with the CH equation, which is based on the Ginzburg–Landau (GL) free energy expansion in terms of a phase separation local order parameter $u(\mathbf{r}, T)$, which is a function of position and temperature T:

$$f(u) = \frac{1}{2}\varepsilon|\nabla u|^2 + V_{GL}(u, T), \tag{1}$$

where $V_{GL}(u, T) = -\alpha[T_{PS} - T]u^2/2 + B^2u^4/4 + ...$ is a double-well potential that characterizes the electronic phase separation below $T_{PS} \approx T^*(p)$ and $T^*(p)$ is the pseudogap temperature [27,28]. We used α and $B = 1$ here but they are usually used to control the CO pattern, and ε controls the spatial separation of the charge-segregated patches. The CH equation can be written in the form of the following continuity equation for the local GL free energy current density $\mathbf{J} = -M\nabla^2((\partial f/\partial u)$ [29]:

$$\frac{\partial u}{\partial t} = -\nabla \mathbf{J} = -M\nabla^2\left[\varepsilon\nabla^2 u + \frac{\partial V_{GL}}{\partial u}\right], \tag{2}$$

where M is the order parameter mobility that sets the time scale. To solve this equation, we used a time-dependent [17,18,20] conserved order parameter associated with local electronic density, $p(\mathbf{r}) = \mathrm{A}u(\mathbf{r}) + p$, where A controls the CO amplitude of oscillation. A is 0.00005 to $\Delta p \approx 10^{-3-4}$ variations around p, like in typical YBCO systems [30]. All the simulations here used $\delta t = 700$ time steps, and we dropped the dependence of t on $u(\mathbf{r})$ and on $V_{GL}(u, T) \equiv V_{GL}(\mathbf{r}, T)$. We assumed that overdoped compounds also have such small charge oscillations Δp that, together with metallic conductivity, they would be almost undetectable.

Figure 1a shows the density distribution $p(\mathbf{r})$ for $p = 0.16$ with hole-rich (red domains) and hole-poor (blue domains) at $T \sim 0$ K. The anisotropic checkerboard-like pattern also favors anisotropic conduction along the easy axis at $\pm 45^\circ$ or $\pm 135^\circ$, which may be an approximated explanation of the transverse voltages measured in [3] from low temperature to room temperature, suggesting that the CO transition may start much above T^*. Figure 1b shows the $T \sim 0$ K free energy map $V_{GL}(\mathbf{r})$ derived from the same $u(\mathbf{r})$ simulation. It is important to note that the domains in blue correspond to both hole-rich and hole-poor regions. To model the observed broadening and the intensity loss of the modulated dynamical spin correlations [6,7,31], we slightly increased ε with p.

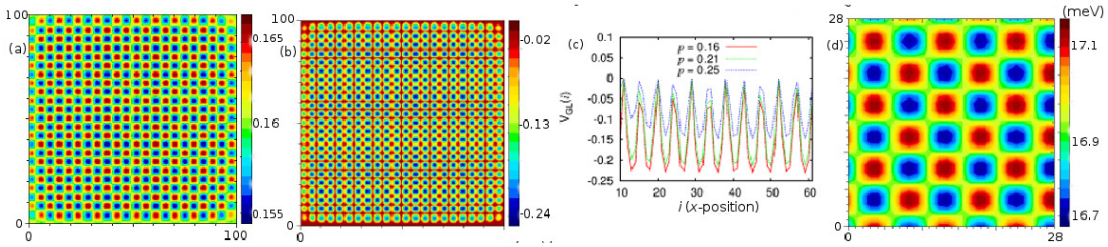

Figure 1. (**a**) Low-temperature Cahn–Hilliard (CH) electronic density $p(\mathbf{r})$ simulation that mimics the measured Q_{CO} for the average charge density $p = 0.16$ with $\Delta p \sim 10^{-3}$. (**b**) From the same simulation, the corresponding free energy potential $V_{GL}(\mathbf{r})$ on a square lattice of 100×100 unit cells (GL: Ginzburg–Landau). (**c**) The spatial dependence of the free energy potential $V_{GL}(\mathbf{r})$ along a straight line in the center of the $p(\mathbf{r})$ simulations of three different dopings. (**d**) The low-temperature d-wave pairing potential $\Delta_d(\mathbf{r})$ on a single domain over a 28×28 unit cell area in $p(\mathbf{r})$. The average $\langle \Delta_d(\mathbf{r}) \rangle$ is 16.9 meV.

Accordingly, Figure 1c shows $V_{GL}(x)$ along the x-direction for $p = 0.16, 0.21$, and 0.25, where the amplitudes decreased with p to mimic the broader peaks in the dynamical spin measurements [6,7,31]. The main idea of our model is that the $V_{GL}(\mathbf{r}, T)$ modulations shown in Figure 1c create regions with alternating charge probability domains or CDWs that promote local SC amplitudes. It was shown by high-energy X-ray diffraction [32] that the observed CDWs also produce atomic displacements with the same modulations, which is a direct experimental demonstration of the electron–phonon coupling. This experiment on single-crystal YBCO, considered the cleanest cuprate, validates the early proposal by A. Muller that strong electron lattice interaction with the formation of polaronic states plays a key role in the high superconductivity of doped perovskites [33]. In La-based superconductors, the connection between inhomogeneous charge states and lattice fluctuations was observed by extended X-ray absorption fine structure (EXAFS) through the Debye–Waller factor of the Cu–O bonds. From these data, the polaronic distortion order parameter across the charge stripe ordering temperature was extracted [34,35]. The results are supported by a temperature-dependent Cu K-edge X-ray absorption near edge structure (XANES) revealing a particular change in the local lattice displacements at the charge stripe ordering. The experimental Cu K-edge XANES results are well reproduced by full multiple scattering calculations including different distortions of the CuO plane showing particular lattice displacements which are consistent with the EXAFS results [36,37].

The isotopic effect at the ordering temperature [38–40] of polaron stripes [41] has also provided compelling evidence that local lattice fluctuations and given experimental support for the polaronic proposal of Alex Muller [33]. The fact that the size of the SC coherence lengths are generally less than λ_{CO} also suggests that valence electrons form lattice-induced Cooper pairs in CO domains.

Therefore, the strength of the attractive two-body SC interaction is assumed to be scaled by the spatial average $\langle V_{GL}(p, T) \rangle \equiv \sum_i^N V_{GL}(r_i, p, T)/N$, where N is the number of unit cells in the CuO plane. An indication of this proportionality was extracted by comparing the results of the experiment of Poccia et al. [42]. They controlled the degree of oxygen ordering by tuning the time t of X-ray irradiation in optimally doped La_2CuO_{4+y} and subsequently measured the SC critical temperature $T_c(t)$, which increased with t up to a saturation limit. We interpreted their results with nδt simulation time and $\langle V_{GL}(p, n\delta t) \rangle$ proportional to the SC interaction in the self-consistent calculations [18]. We found that taking time steps of 2000 δt in the CH simulations was equivalent to 0.1 h of X-ray irradiation, and we could closely reproduce the $T_c(t)$ evolution with time, as described in [18].

The local SC amplitude map $\Delta_d(\mathbf{r})$ was calculated via self-consistent Bogoliubov–deGennes (BdG) calculations [17–20] based on a Hubbard Hamiltonian with an attractive potential scaled by $\langle V_{GL}(p, T) \rangle$. The GL potential average $\langle V_{GL}(p, T) \rangle$ has no dimension and it was necessary to multiply it by a constant in order to define the attractive pairing potential $\langle V_{GL}(p, T) \rangle$ in eV units. We adjusted

the $T \sim 0$ K $\langle V_{\rm GL}(p_0 = 0.16, T)\rangle$ to reproduce the measured SC gap $\Delta_{\rm sc}(p_0 = 0.16)$. Once this was done, all the other $\langle V_{\rm GL}(p)\rangle$ followed from their $\langle V_{\rm GL}(p)\rangle / \langle V_{\rm GL}(p_0)\rangle$ ratio. The $T \sim 0$ K calculation with $\langle V_{\rm GL}(p)\rangle = 0.234$ eV yielded $\langle \Delta_d(\mathbf{r}, p_0 = 0.16)\rangle \sim 16.9$ meV, which is close to the measured LSCO nodal gap ($\langle \Delta_0(p_0 = 0.16)\rangle \sim 16 - 17$ meV) [43].

A typical SC $\Delta_d(\mathbf{r}, p = 0.16)$ result in contour map format is shown in Figure 1d. $\Delta_d(\mathbf{r}, p)$ and $p(\mathbf{r})$ are plotted with different scales, but the charge and pairing amplitude density modulations had the same $\lambda_{\rm CO}$. Figure 2a shows $\langle \Delta_d(p, T)\rangle$, and it is clear that all SC amplitudes remained finite above $T_{\rm c}$, in agreement with measurements of persisting SC correlations above $T_{\rm c}$ [22,23,28,44].

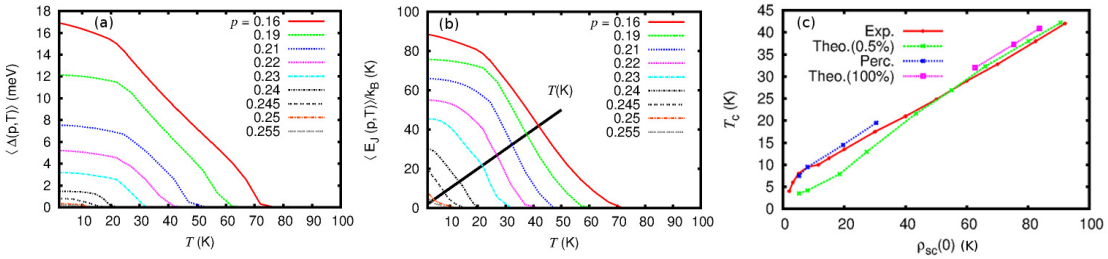

Figure 2. The calculations of $\langle \Delta_d(T)\rangle$, $\rho_{\rm sc}(T)$, and $T_{\rm c}$. (**a**) $\langle \Delta_d(p, T)\rangle$ for several compounds. (**b**) The same for $\langle E_{\rm J}(p, T)\rangle$. (**c**) The main result, the values of $\rho_{\rm sc}(p, 0)$ and $T_c(p)$ derived directly from $E_{\rm J}$ (green) with the experimental results in [1] (red). In the far overdoping region, the metallic behavior favors the SC percolation from the charge domains (blue). The calculations with large (100%) charge density wave (CDW) amplitude (pink) yield lower $\langle E_{\rm J}(p, T)\rangle$, and $T_{\rm c}$.

3. Discussion

Since our calculations rely heavily on the existence of CO or CDW, which is not widely observed in overdoped samples (other than in [6,7]), we studied the case of very small (i.e., $\Delta p = 10^{-4}$) relative electronic modulations, as well as large oscillations for comparison. The calculations with only $\Delta p = 0.0005\%$ variation in the charge density yielded essentially the same $\langle \Delta_d(p, T)\rangle$ of the case studied here with 0.5% charge oscillation. The reason for this is that the free energy average $\langle V_{\rm GL}\rangle$ is independent of the charge amplitude. Therefore, we draw the important conclusion that the SC properties depend very little on the charge amplitude but—as shown elsewhere [20]—they depend strongly on the wave vector of the charge order $\lambda_{\rm CO}$.

When the temperature decreases, the two-component SC order parameter $(\Delta_d(r_i), \theta_i)$ develops at each charge domain like in granular superconductors [26]. The $\Delta_d(\mathbf{r})$ distribution in Figure 1d resembles a multiple-grain superconductor. In this case, the interface between two neighbor grains gives rise to a Josephson junction with an energy $E_{\rm J}(r_{ij})$ between grains i and j that is proportional to the local superfluid density $\rho_{\rm sc}$ [24]. Therefore, cuprates may be regarded as an array of these junctions. For a d-wave superconductor in single crystals, it is sufficient to use the s-wave relation for the average Josephson coupling energy [17,18,20]:

$$\langle E_{\rm J}(p, T)\rangle = \frac{\pi h \langle \Delta_d(p, T)\rangle}{2e^2 R_{\rm n}(p)} \tanh\Big[\frac{\langle \Delta_d(p, T)\rangle}{2k_{\rm B}T}\Big]. \quad (3)$$

$R_{\rm n}(p)$ is proportional to the normal-state in-plane resistivity $\rho_{ab}(p)$ that was also measured in [1], which is crucial to our approach. We used the values of $\langle \Delta_d(p, T)\rangle$ plotted in Figure 2a to derive $\langle E_{\rm J}(p, T)\rangle$. Figure 2b shows $\langle E_{\rm J}(p, T)\rangle$ vs. T. $R_{\rm n}(p_0 = 0.16)$ was scaled to yield $T_c \sim 42$ K and all the other $R_{\rm n}(p)$ follow from their experimental ratio. The derived $R_{\rm n}(p)$ by this procedure closely follows the measured [1] $\rho_{\rm n}(p) \sim \rho_{ab}(p)$ plotted in [1] (extended data Figure 8). We emphasize that $R_{\rm n}(p_0 = 0.16)$ and $\langle \Delta_d(\mathbf{r}, p_0 = 0.16)\rangle$ contain the only two adjustable parameters of our theory, from which we derived the entire phase diagram; that is, $\rho_{\rm sc}(0)$, $\langle \Delta_d(\mathbf{r})\rangle$, and $\langle E_{\rm J}\rangle$ to any hole doping p and T, and especially $T_c(p)$.

Long-range SC phase coherence between the CO or CDW nano-domains occurs when $k_B T \approx \langle E_J(p,T)\rangle$. Figure 2b shows the calculations of $k_B T \approx \langle E_J(p,T)\rangle/k_B$, and the bulk critical temperature $T_c(p)$ is given by the intersection with the temperature T black line. The Josephson coupling yields the superfluid density [24] because $\rho_{sc}(p,0) \sim \langle E_J(p,T \sim 0\mathrm{K})\rangle$. Thus, from the curves $\langle E_J(p,T)\rangle$ vs. T we simultaneously derived $T_c(p)$ and $\rho_{sc}(p,0)$.

We plot our main result, the calculated $T_c(p)$ vs. $\rho_{sc}(p,0)$ in Figure 2c together with the measurements of Bozovic et al. [1]. We also plot three points with large charge amplitude ($\Delta p = 100\%$ modulations with A = 1), which demonstrate that increasing the charge amplitude Δp had very little effect on T_c and ρ_{sc}. The linear relation between $\rho_{sc}(0)$ and T_c was robust to all the different possible charge modulations. Beyond $p = 0.24$, the measured residual resistivity became very small [1], and the weak links broke down, allowing quasiparticle current. The Josephson coupling energy vanished, and the charge domains all had the same phase. In this regime, the system crossed over from a granular superconductor to a single disordered superconductor, and the resistivity transition occurred by percolation and proximity effect. Under these conditions, $T_c(p)$ coincided with the onset of $\langle \Delta_d(p,T)\rangle$ shown in Figure 2a and represented by the blue points and line in Figure 2c for the range of $p = 0.24$–0.26.

4. Conclusions

We verified that LSCO films are well-described by mesoscopic grains with charge modulation λ_{CO}, similar to a granular superconductor. Our calculations showed that the linear $\rho_{sc}(0)$ vs. T_c scaling relation was robust even when the relative charge variations in CO or CDW were as small as $\sim 10^{-4}$. The decrease of $\rho_{sc}(0)$ with p is also consistent with another interpretation derived from EXAFS studies [36,37], suggesting that electron–lattice interaction decreases with increasing doping. This behavior was argued to be closely related to the evolving anomalous local CuO distortion and charge inhomogeneity with doping, even into the overdoped region of LSCO compounds [45]. These experiments and our calculations on the $\rho_{sc}(0)$ vs. T_c experiment provide more support for the polaronic proposal of Alex Muller [33].

Recently, this scenario has also been supported by the investigations on new functional solids by new advanced methods [46,47]. The complexity is driven by cooperative effects of the self organization of dopants discussed in detail in a Special Issue [48], the pseudo Jahan Teller effect involving multiple orbitals [49,50], and local lattice tilts [51]. These results are currently a hot topic, since the strong electron–phonon interaction in complex multi-band materials in extreme conditions near lattice instabilities is emerging as a key mechanism in high-temperature superconductor hydrides [52,53] showing anomalous isotope effect [54,55].

Funding: This research received no external funding.

Acknowledgments: I thank the Brazilian agencies CNPq and FAPERJ for partial support.

Conflicts of Interest: The author declares no conflict of interest.

References

1. Božović, I.; He, X.; Wu, J.; Bollinger, A.T. Dependence of the critical temperature in overdoped copper oxides on superfluid density. *Nature* **2016**, *536*, 309–311. [CrossRef]
2. Torchinsky, D.H.; Mahmood, F.; Bollinger, A.T.; Božović, I.; Gedik, N. Fluctuating charge-density waves in a cuprate superconductor. *Nat. Mater.* **2013**, *12*, 387–391. [CrossRef]
3. Wu, J.; Bollinger, A.T.; He, X.; Božović, I. Spontaneous breaking of rotational symmetry in copper oxide superconductors. *Nature* **2017**, *547*, 432–435. [CrossRef]
4. Comin, R.; Damascelli, A. Resonant X-Ray Scattering Studies of Charge Order in Cuprates. *Ann. Rev. Condens. Mat. Phys.* **2016**, *7*, 369. [CrossRef]

5. Dean, M.P.M.; Dellea, G.; Springell, R.S.; Yakhou-Harris, F.; Kummer, K.; Brookes, N.B.; Liu, X.; Sun, Y.-J.; Strle, J.; Schmitt, T.; et al. Persistence of magnetic excitations in $La_{2-x}Sr_xCO_4$ from the undoped insulator to the heavily overdoped non-superconducting metal. *Nat. Mater.* **2013**, *12*, 1019–1023. [CrossRef]
6. Yamada, K.; Lee, C.H.; Kurahashi, K.; Wada, J.; Wakimoto, S.; Ueki, S.; Kimura, H.; Endoh, Y.; Hosoya, S.; Shirane, G.; et al. Doping dependence of the spatially modulated dynamical spin correlations and the superconducting-transition temperature in $La_{2-x}Sr_xCuO_4$. *Phys. Rev. B* **1998**, *57*, 6165–6172. [CrossRef]
7. Tranquada, J.M.; Axe, J.D.; Ichikawa, N.; Moodenbaugh, A.R.; Nakamura, Y.; Uchida, S. Coexistence of, and Competition between, Superconductivity and Charge-Stripe Order in $La_{1.6-x}Nd_{0.4}Sr_xCuO_4$. *Phys. Rev. Lett.* **1997**, *78*, 338–341. [CrossRef]
8. Mahmood, F.; He, X.; Božović, I.; Armitage, N.P. Locating the Missing Superconducting Electrons in the Overdoped Cuprates $La_{2-x}Sr_xCuO_4$. *Phys. Rev. Lett.* **2019**, *122*, 027003. [CrossRef]
9. Lee-Hone, N.R.; Dodge, J.S.; Broun, D.M. Disorder and superfluid density in overdoped cuprate superconductors. *Phys. Rev. B* **2017**, *96*, 024501. [CrossRef]
10. Vojta, M. Superconducting charge-ordered states in cuprates. *Phys. Rev. B* **2002**, *66*, 104505. [CrossRef]
11. Ortix, C.; Lorenzana, J.; Di Castro, C. Coulomb-Frustrated Phase Separation Phase Diagram in Systems with Short-Range Negative Compressibility. *Phys. Rev. Lett.* **2008**, *100*, 246402. [CrossRef]
12. Nie, L.; Maharaj, A.V.; Fradkin, E.; Kivelson, S.A. Vestigial nematicity from spin and/or charge order in the cuprates. *Phys. Rev. B* **2017**, *96*, 085142. [CrossRef]
13. Okamoto, S.; Sénéchal, D.; Civelli, M.; Tremblay, A.M.S. Dynamical electronic nematicity from Mott physics. *Phys. Rev. B* **2010**, *82*, 180511. [CrossRef]
14. Ghiringhelli, G.; Le Tacon, M.; Minola, M.; Blanco-Canosa, S.; Mazzoli, C.; Brookes, N.B.; De Luca, G.M.; Frano, A.; Hawthorn, D.G.; He, F.; et al. Long-range incommensurate charge fluctuations in $(Y,Nd)Ba_2Cu_3O_{(6+x)}$. *Science* **2012**, *337*, 821–825. [CrossRef]
15. Campi, G.; Bianconi, A.; Poccia, N.; Bianconi, G.; Barba, L.; Arrighetti, G.; Innocenti, D.; Karpinski, J.; Zhigadlo, N.D.; Kazakov, S.M.; et al. Inhomogeneity of charge-density-wave order and quenched disorder in a high-Tc superconductor. *Nature* **2015**, *525*, 359–362. [CrossRef]
16. de Mello, E.; da Silveira Filho, O.T. Numerical study of the Cahn–Hilliard equation in one, two and three dimensions. *Physica A* **2005**, *347*, 429–443. [CrossRef]
17. de Mello, E.V.L.; Kasal, R.B.; Passos, C.A.C. Electronic phase separation transition as the origin of the superconductivity and pseudogap phase of cuprates. *J. Phys. Condens. Matt.* **2009**, *21*, 235701. [CrossRef]
18. de Mello, E.V.L. Disordered-based theory of pseudogap, superconducting gap, and Fermi arc of cuprates. *Eur. Phys. Lett.* **2012**, *99*, 37003. [CrossRef]
19. de Mello, E.V.L.; Sonier, J.E. Charge segregation model for superconducting correlations in cuprates above T c. *J. Phys. Condens. Matt.* **2014**, *26*, 492201. [CrossRef]
20. de Mello, E.V.L.; Sonier, J.E. Superconducting correlations induced by charge ordering in cuprate superconductors and Fermi-arc formation. *Phys. Rev. B* **2017**, *95*, 184520. [CrossRef]
21. Cahn, J.W.; Hilliard, J.E. Free Energy of a Nonuniform System. I. Interfacial Free Energy. *J. Chem. Phys.* **1958**, *28*, 258. [CrossRef]
22. Corson, J.; Mallozzi, R.; Orenstein, J. Vanishing of phase coherence in underdoped $Bi_2Sr_2CaCu_2O_{8+x}$. *Nature* **1999**, *406*, 221–223. [CrossRef]
23. Xu, Z.A.; Ong, N.P.; Wang, Y.; Kakeshita, T.; Uchida, S. Vortex-like excitations and the onset of superconducting phase fluctuation in underdoped $La_{2-x}Sr_xCuO_4$. *Nature* **2000**, *406*, 486–488. [CrossRef]
24. Spivak, B.I.; Kivelson, S.A. Negative local superfluid densities: The difference between dirty superconductors and dirty Bose liquids. *Phys. Rev. B* **1991**, *43*, 3740–3743. [CrossRef]
25. Lang, K.M.; Madhavan, V.; Hoffman, J.E.; Hudson, E.W.; Eisaki, H.; Uchida, S.; Davis, J.C. Imaging the granular structure of high-Tc superconductivity in underdoped $Bi_2Sr_2CaCu_2O_{8+d}$. *Nature* **2002**, *415*, 412–416. [CrossRef]
26. Imry, Y.; Strongin, M.; Homes, C.C. $n_s - T_c$ Correlations in Granular Superconductors. *Phys. Rev. Lett.* **2012**, *109*, 067003. [CrossRef]
27. Wang, Y.; Li, L.; Ong, N.P. Nernst effect in high-T_c superconductors. *Phys. Rev. B* **2006**, *73*, 024510. [CrossRef]
28. Gomes, K.K.; Pasupathy, A.N.; Pushp, A.; Ono, S.; Ando, Y.; Yazdani, A. Visualizing pair formation on the atomic scale in the high-Tc superconductor $Bi_2Sr_2CaCu_2O_{8+\delta}$. *Nature* **2007**, *447*, 569–572. [CrossRef]
29. Bray, A. Theory of phase-ordering kinetics. *Adv. Phys.* **1994**, *43*, 357–459. [CrossRef]

30. Kharkov, Y.A.; Sushkov, O.P. The amplitudes and the structure of the charge density wave in YBCO. *Sci. Rep.* **2016**, *6*, 34551. [CrossRef]
31. Hücker, M.; Christensen, N.B.; Holmes, A.T.; Blackburn, E.; Forgan, E.M.; Liang, R.; Bonn, D.A.; Hardy, W.N.; Gutowski, O.; Zimmermann, M.V.; et al. Competing charge, spin, and superconducting orders in underdoped $YBa_2Cu_3O_y$. *Phys. Rev. B* **2014**, *90*, 1–11. [CrossRef]
32. Chang, J.; Blackburn, E.; Holmes, T.; Christensen, N.B.; Larsen, J.; Mesot, J.; Liang, R.; Bonn, D.A.; Hardy, W.N.; Watenphul, A.; et al. Direct observation of competition between superconductivity and charge density wave order in $YBa_2Cu_3O_{6.67}$. *Nat. Phys.* **2012**, *8*, 871–876. [CrossRef]
33. Bussmann-Holder, A.; Müller, K.A. *Superconductivity in Complex Systems*; Springer: Berlin/Heidelberg, Germany, 2005.
34. Saini, N.L.; Oyanagi, H.; Wu, Z.; Bianconi, A. Lattice fluctuations and inhomogeneous charge states of high-Tc superconductors Supercondors. *Sci. Technol.* **2002**, *15*, 439–449. [CrossRef]
35. Saini, N.L.; Oyanagi, H.; Ito, T.; Scagnoli, V.; Filippi, M.; Agrestini, S.; Bianconi, A. Lattice fluctuations and inhomogeneous charge states of high-Tc superconductors Supercondors. *Eur. Phys. J. B Condens. Matt. Complex Syst.* **2003**, *36*, 75–80. [CrossRef]
36. Saini, N.L.; Oyanagi, H.; Scagnoli, V.; Ito, T.; Oka, K.; Bianconi, A. Different temperature-dependent local displacements in the underdoped and overdoped $La_{2-x}Sr_xCuO_4$system. *EPL* **2003**, *63*, 125–131. [CrossRef]
37. Saini, N.L.; Oyanagi, H.; Scagnoli, V.; Ito, T.; Oka, K.; Bianconi, A. Study of Temperature Dependent Local Structure by Polarized Cu K-edge EXAFS Measurements on $La_{2-x}Sr_xCuO4$ (x=0.105. 0.13. 0.20). *J. Phys. Soc. Jpn* **2003**, *72*, 829–834. [CrossRef]
38. Lanzara, A.; meng Zhao, G.; Saini, N.L.; Bianconi, A.; Conder, K.; Keller, H.; Müller, K.A. Oxygen-isotope shift of the charge-stripe ordering temperature in $La_{2-x}Sr_xCuO_4$from x-ray absorption spectroscopy. *J. Phys. Condens. Matt.* **1999**, *11*, L541–L546. [CrossRef]
39. Bendele, M.; von Rohr, F.; Guguchia, Z.; Pomjakushina, E.; Conder, K.; Bianconi, A.; Simon, A.; Bussmann-Holder, A.; Keller, H. Evidence for strong lattice effects as revealed from huge unconventional oxygen isotope effects on the pseudogap temperature in $La_{2-x}Sr_xCuO_4$. *Phys. Rev. B* **2017**, *95*, 014514. [CrossRef]
40. Bussmann-Holder, A.; Keller, H.; Khasanov, R.; Simon, A.; Bianconi, A.; Bishop, A.R. Isotope and interband effects in a multi-band model of superconductivity. *New J. Phys.* **2011**, *13*, 093009. [CrossRef]
41. Kusmartsev, F.V.; Castro, D.D.; Bianconi, G.; Bianconi, A. Transformation of strings into an inhomogeneous phase of stripes and itinerant carriers. *Phys. Lett. A* **2000**, *275*, 118–123. [CrossRef]
42. Poccia, N.; Fratini, M.; Ricci, A.; Campi, G.; Barba, L.; Vittorini-Orgeas, A.; Bianconi, G.; Aeppli, G.; Bianconi, A. Evolution and control of oxygen order in a cuprate superconductor. *Nat. Mater.* **2011**, *10*, 12. [CrossRef]
43. Yoshida, T.; Hashimoto, M.; Vishik, I.M.; Shen, Z.X.; Fujimori, A. Pseudogap, Superconducting Gap, and Fermi Arc in High-Tc Cuprates Revealed by Angle-Resolved Photoemission Spectroscopy. *J. Phys. Soc. Jpn* **2012**, *81*, 011006. [CrossRef]
44. Dubroka, A.; Rössle, M.; Kim, K.W.; Malik, V.K.; Munzar, D.; Basov, D.N.; Schafgans, A.A.; Moon, S.J.; Lin, C.T.; Haug, D.; et al. Evidence of a precursor superconducting phase at temperatures as high as 180 K in $RBa_2Cu_3O_{(7-\delta)}$ (R=Y,Gd,Eu) superconducting crystals from infrared spectroscopy. *Phys. Rev. Lett.* **2011**, *106*, 1–4. [CrossRef]
45. Deutcher, G. *From Granular Superconductivity to High Tc in High-Tc Copper Oxide Superconductors and Related Novel Materials*; Springer: Berlin/Heidelberg, Germany, 2017.
46. Shamoto, S.i. Local Structure of Functional Solids. *J. Phys. Soc. Jpn* **2019**, *88*, 081008. [CrossRef]
47. Campi, G.; Bianconi, A. Evolution of Complexity in Out-of-Equilibrium Systems by Time-Resolved or Space-Resolved Synchrotron Radiation Techniques. *Condense. Matt.* **2019**, *4*, 32. [CrossRef]
48. Jarlborg, T.; Bianconi, A. Multiple Electronic Components and Lifshitz Transitions by Oxygen Wires Formation in Layered Cuprates and Nickelates. *Condense. Matt.* **2019**, *4*, 15. [CrossRef]
49. Oleś, A.M.; Wohlfeld, K.; Khaliullin, G. Orbital Symmetry and Orbital Excitations in High-Tc Superconductors. *Condense. Matt.* **2019**, *4*, 46. [CrossRef]
50. Mou, Y.; Liu, Y.; Tan, S.; Feng, S. Doping and momentum dependence of coupling strength in cuprate superconductors. *arXiv* **2019**, arXiv:1903.00803.

51. Gavrichkov, V.A.; Shan'ko, Y.; Zamkova, N.G.; Bianconi, A. Is There Any Hidden Symmetry in the Stripe Structure of Perovskite High-Temperature Superconductors? *J. Phys. Chem. Lett.* **2019**, *10*, 1840–1844. [CrossRef]
52. Bianconi, A.; Jarlborg, T. Superconductivity above the lowest Earth temperature in pressurized sulfur hydride. *EPL* **2015**, *112*, 37001. [CrossRef]
53. Mozaffari, S.and Sun, D.; Minkov, V.S.; Knyazev, D.; Betts, J.B.; Einaga, M.; Balakirev, F.F. Superconducting Phase-Diagram of H_3S under High Magnetic Fields. *arXiv* **2019**, arXiv:1901.11208.
54. Jarlborg, T.; Bianconi, A. Breakdown of the Migdal approximation at Lifshitz transitions with giant zero-point motion in the H3S superconductor. *Sci. Rep.* **2016**, *6*, 24816. [CrossRef]
55. Villa-Cortés, S.; Baquero, R. The thermodynamics and the inverse isotope effect of superconducting palladium hydride compounds under pressure. *J. Phys. Chem. Solids* **2018**, *123*, 371–377. [CrossRef]